

KOSZALIN UNIVERSITY OF TECHNOLOGY

**RESEARCH AND MODELLING  
IN CIVIL ENGINEERING  
2019**

Edited by  
Jacek Katzer, Krzysztof Cichocki and Jacek Domski

KOSZALIN 2019

MONOGRAPH NO 366  
FACULTY OF CIVIL ENGINEERING,  
ENVIRONMENTAL AND GEODETIC SCIENCES

ISSN 0239-7129

ISBN 978-83-7365-525-6

Chairman of the University Editorial Board

*Zbigniew Danielewicz*

Editors

*Jacek Katzer, Krzysztof Cichocki and Jacek Domski*

*Koszalin University of Technology, Poland*

Reviewers

*Jacek Gołaszewski – Silesian University of Technology, Poland*

*Wojciech Sumelka – Poznań University of Technology, Poland*

Technical editor

*Czesław Suchocki*

Website editor

*Mariusz Ruchwa*

Linguistic consultations

*Ewa Sokołowska-Katzer*

Typesetting

*Czesław Suchocki*

Cover design

*Tadeusz Walczak*

[www.cecem.eu](http://www.cecem.eu)

© Copyright by Koszalin University of Technology Publishing House

Koszalin 2019

*This work is licensed under a Creative Commons Attribution-NonCommercial-ShareAlike  
4.0 International License.*



KOSZALIN UNIVERSITY OF TECHNOLOGY PUBLISHING HOUSE

75-620 Koszalin, Raławicka 15-17, Poland

---

Koszalin 2019, 1<sup>st</sup> edition, publisher's sheet 8,23, circulation 120 copies

Printing: INTRO-DRUK, Koszalin, Poland

## **Table of contents**

<b>1. Thermally loaded concrete specimens: fractal dimensions of fracture surface and mechanical fracture parameters .....</b>	<b>7</b>
<b>2. Contribution to comparison of methods for the investigation of chloride ingress related resistance.....</b>	<b>31</b>
<b>3. Requirements for BIM model.....</b>	<b>41</b>
<b>4. Comparative study of Building Law in Poland and Russian Federation.....</b>	<b>55</b>
<b>5. Numerical analysis of a semi-circular disc with an angled crack loaded in mixed-mode .....</b>	<b>71</b>
<b>6. Methodology for static analysis of pre-stressed plane cable systems .....</b>	<b>85</b>
<b>7. A UAV-based 3D model for building condition monitoring .....</b>	<b>107</b>
<b>8. Creating a web application to calculate predicted exploitative resistance to frost .....</b>	<b>121</b>
<b>9. The effect of steel fibres on selected properties of new generation of concrete .....</b>	<b>133</b>

# 1. Thermally loaded concrete specimens: fractal dimensions of fracture surface and mechanical fracture parameters

Iva Rozsypalová<sup>1</sup>, Tomáš Trčka<sup>2</sup>, Petr Frantík<sup>1</sup>, Hana Šimonová<sup>1</sup>,  
Barbora Svobodová<sup>1</sup>, Petr Daněk<sup>1</sup>, Zbyněk Keršner<sup>1,3</sup>

<sup>1</sup>Brno University of Technology, Faculty of Civil Engineering, Brno, Czech Republic,  
iva.rozsypalova@vutbr.cz, orcid.org/0000-0003-3109-3820, kitnarf@centrum.cz, orcid.org/0000-0003-0141-2966, simonova.h@vutbr.cz, orcid.org/0000-0003-1537-6388, BaraKory@seznam.cz, orcid.org/0000-0001-7922-0847, petr.danek@vutbr.cz, orcid.org/0000-0001-8489-9452, kersner.z@fce.vutbr.cz, orcid.org/0000-0003-4724-6166

<sup>2</sup>Brno University of Technology, Faculty of Electrical Engineering and Communication, Brno, Czech Republic, xtrcka03@gmail.com, orcid.org/0000-0002-3704-9532

**Abstract:** The chapter deals primarily with the fractal dimension of fracture surfaces of fractured concrete specimens after thermal loading. These specimens were obtained from experimental concrete panels after extensive fire experiments. The panels were exposed on one side to heat from a furnace at nominal maximum temperatures of 550, 600, 800 and 1000 °C. Reference specimens unexposed to heat load were also tested. Specimens with nominal dimensions of 100 × 100 × 400 mm and a 33 mm central edge notch were tested in the three-point bending configuration; load versus displacement diagrams were recorded, corrected and evaluated. Each set contained 4 specimens, and a total of 20 specimens were processed. The following basic mechanical fracture parameters were assessed: modulus of elasticity, effective fracture toughness and specific fracture energy. The fracture surfaces (ligaments) of all tested specimens were analyzed in detail after the above-mentioned three-point bending tests. The ligaments were scanned via a 2D laser profilometer and the fractal dimension of selected sections of these surfaces was measured. The fractal dimension of the fracture surface sections was estimated using the walking divider method. Finally, the chapter presents the correlation among the fractal dimensions, the temperatures in the concrete at different distances from the heated side and the previously obtained and above-mentioned mechanical fracture parameters.

**Keywords:** concrete, high-temperature, testing, material properties, fractals

## 1.1. Introduction

Cement-based composites, with concrete as their main representative, rank among the most widely used building materials. Although concrete is traditionally considered to be fire-resistant, thermal loading affects the whole range of its mechanical, transport and other properties – see e.g. (Aïtcin and Mindess, 2011), (Nevile, 2011). Consequently, the monitoring of many aspects of fire-resistance – especially that of load-bearing reinforced and pre-stressed concrete structures – has long been a topical issue for research, recommendations, and codes – see e.g. (Purkiss and Li, 2011), (Wang *et al.*, 2013), (RILEM TC 129-MHT, 1997), (Eurocode EN 1991-1-2:2002/AC, 2013). This chapter is focused on a specific investigation regarding this issue: selected specimens were sawn from thermally loaded experimental plain concrete panels and submitted to fracture tests, after which the fractal dimensions of the selected fracture surface sections were evaluated. The results of this research also include observed correlations between fractal dimension values and selected (previously determined) mechanical fracture parameters of thermally loaded concrete.

## 1.2. Background: fracture complexity

Concrete, mortar, rock, ceramics, masonry and other building materials exhibit quasi-brittle behaviour; see (Shah *et al.*, 1995), (Bažant and Planas, 1998), etc. Advanced fracture tests performed on these materials are typically focused on the determination of mechanical fracture properties and basic relationships such as fracture toughness, fracture energy, cohesive law, tensile strength, etc. These are usually determined from specimens loaded by controlled increasing displacement at very low velocities. This loading with almost negligible global dynamic effects is known as quasi-static. However, fracture in a quasi-brittle material is a dynamic process and a naturally transient phenomenon with nonlinear characteristics. These characteristics are commonly overlooked or unknown, though their study can have a deep impact on the understanding of fracture processes and can have an effect on the definition and determination of fracture properties.

During the loading of tested specimens, a complex acoustic signal is generated containing information about changes in the inner structure of the stressed material. Nonlinear signal analysis allows, for example, metric entropy not only to estimate the dominant state variables in a loaded system but also to quantify microstructural changes in a material (Carpinteri and Lacidogna, 2008), (Edelman *et al.*, 2017). Material response to dynamic loading can be influenced by low energy periodic excitation. The influence of the generator on the propagation of microcracks or dislocations during loading has not yet been sufficiently investigated, but it is believed that provoked energy release can have a measurable impact on the entire fracture process. Methods of measuring this

nature are being developed together with the search for correlation between the structural characteristics of material and the spectrum of the excitation signal.

Today, the fracture properties of building materials are playing an increasingly important role in their application. Higher quality natural materials and especially artificial composites are now being employed in the construction industry to build structures that are required to be durable and reliable under often unknown critical loads. Thanks to this advance, properties that were previously neglected have come to the foreground.

Classical Fracture Mechanics works in the case of the quantification of parameters characterizing a fracture process with a geometrically simple fracture surface created by the projection of a fracture surface into a plane. However, in reality it is always a more or less rough surface whose properties are lost after projection. That is why Fractal Fracture Mechanics is being developed. It takes the more natural approach of looking at the fracture surface as a fractal set whose generalized dimension forms a new generic attribute of the fracture surface: see (Carpinteri *et al.*, 1999), (Carpinteri *et al.*, 2002), (Carpinteri and Puzzi, 2006), (Alves and Alkimin de Lacerda, 2012) and (Ficker, 2007). The change to viewing the fracture surface in terms of fractal geometry means that it is no longer possible to speak reliably about the fracture area of the fracture surface since its determination is linked to the scale. With increasing detail, the measured approximated area, which is not limited in mathematical terms, grows. The fracture area can then be viewed rather as a projection of the fracture surface into a plane along the propagating crack.

Thanks to the pioneering work of Benoit Mandelbrot (Mandelbrot, 1982), (Mandelbrot *et al.*, 1984), the search for relationships between the geometric properties of fracture surfaces and the mechanical properties of fractured material has begun. The fractal approach has been successfully applied to the brittle fracture of ceramics (Passoja and Amborski, 1978), (Mecholsky *et al.*, 1989), the fracture of metals (Mandelbrot *et al.*, 1984), the fracture of quasi-brittle materials (Carpinteri *et al.*, 1999), (Borodich, 1999), (Mourot *et al.*, 2005), polymers (Kozlov *et al.*, 2004), porous gel (Ficker, 2008), and rocks (Badabagli and Develi, 2003). In this chapter, fracture surface fractality is determined on a set of selected thermally loaded concrete specimens obtained from experimental concrete panels after fire tests.

### **1.3. Material, concrete panels, and fire tests**

A total of 5 large-format concrete slabs (panels) with a nominal size of 2300 × 1300 × 150 mm were produced for extensive fire testing. The formwork was specially constructed from waterproof plywood boards and covered with plastic film to facilitate subsequent un moulding.

To ensure safety during panel testing and handling, it was necessary to reinforce the panels with a welded wire mesh (wire diameter 6 mm, square grid 100 × 100 mm) placed 15 mm from the bottom side of the experimental panels. Subsequently, K-type thermocouples (capable of measuring temperatures ranging from −200 °C to 1250 °C) were installed in order to record the temperatures reached during the fire tests. Each panel was provided with a total of 10 thermocouples located along the longitudinal axis of the panel. Three sensors were installed 10 mm from the bottom side of the panel, three sensors were at the upper side of the panel (here, installation took place after casting), three sensors were in the middle of the panel's thickness (i.e. 75 mm from the bottom side), and additionally one sensor was located at one fourth of the panel's thickness (i.e. 37.5 mm from the bottom side). In the direction of the panel's length, these thermocouples were positioned at the centre (cross-section with four thermocouples) and edges of the considered heated area, i.e. 350 mm from the edges of the panel (cross-sections with three sensors). A detailed scheme of the positions of the thermocouples placed in the experimental panels is shown in Fig. 1.1.

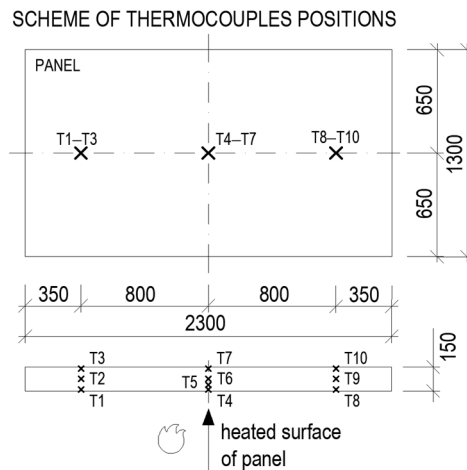


**Fig. 1.1.** Scheme showing the positions of thermocouples T1–T10 in the experimental panels

Standard structural concrete was selected for the concrete mixture used to produce the experimental panels. No modifications were performed to achieve better fire-resistance properties. The panels were made of C30/37 strength class concrete with quartz aggregate (maximum grain size 16 mm). The composition of the fresh concrete mixture is shown in Table. 1.1. After casting, the surface of the specimens was covered with plastic film to prevent water evaporation. When

seven days had passed, the formwork and foil were removed. Then, the panels were un moulded and kept under standard laboratory conditions for another 5 to 6 months, after which the fire tests were carried out.

**Table. 1.1.** Fresh concrete composition

Component	Amount per 1 m <sup>3</sup> [kg]
Cement CEM I 42.5 R	335
Water	170
Sand 0–4	840
Aggregate 8–16	880
Fly ash	50
CX Isoflex 833 Superplasticizer	2.67

The concrete experimental panels were subjected to high temperatures from a gas furnace designed for the testing of building components and structures. The furnace is installed at the AdMaS Science Centre, which belongs to the Faculty of Civil Engineering, Brno University of Technology, Czech Republic. The panels were positioned on the top of the furnace (see Fig. 1.2.), thereby heating them on one side. The unheated sides of the panel were left to cool spontaneously.

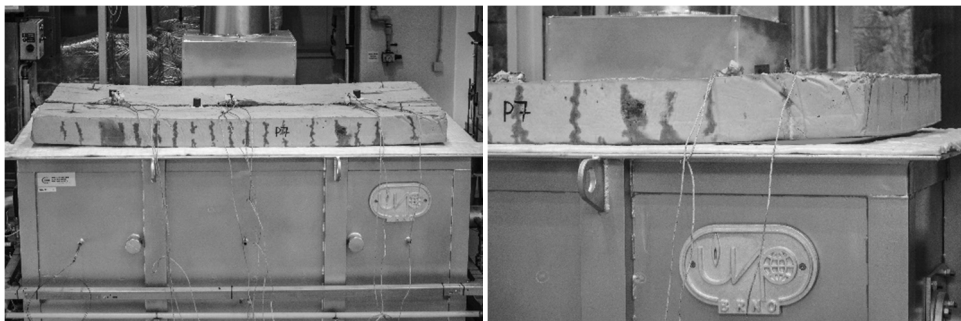


**Fig. 1.2.** The gas furnace designed for studying the behaviour of materials exposed to high temperatures at the AdMaS Science Centre during the fire testing of panel P7, which was heated up to a maximum nominal temperature of 1000 °C; detail on the right

The exposure of panels to high temperatures can be divided into two phases. First, the panels were loaded by a rapid rise in temperature from the furnace, where the individual nominal maximum temperatures were 550, 600, 800, and 1000 °C (corresponding panel designations P1, P2, P3, and P7, respectively; P4 was a reference panel without thermal loading). The temperature increase in the furnace was controlled according to the ISO 834 standardized curve specified in EN 1992-1-2 until the desired temperature level was reached. In the second phase, the temperature in the furnace was maintained at the maximum nominal

temperature for 60 minutes. After the second phase had finished, the furnace was turned off and the panels were left on the top of the furnace to cool spontaneously to room temperature. Records of the temperatures measured in the gas furnace during each fire test are shown in Fig. 1.3. Part of the evaluation of these fire experiments can be found in, for example, (Rozsypalová *et al.*, 2018).

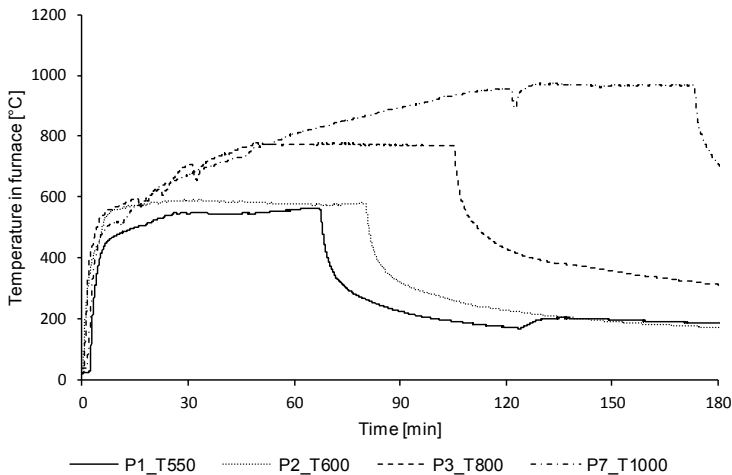


**Fig. 1.3.** Graph of the temperatures measured in the furnace during the fire testing of experimental panels P1, P2, P3, and P7

#### 1.4. The specimens sawn from panels for fracture testing, and their basic mechanical fracture parameters

The four specimens intended for the fracture experiments (Rozsypalová *et al.*, 2017) were cut from the central (most thermally loaded) part of each of the above-mentioned experimental panels – see the scheme in Fig. 1.4. These specimens were labelled A, B, C and D (with nominal dimensions of 100 × 100 × 400 mm). The specimens were subsequently provided with an initial central edge notch cut to a depth of approximately 1/3 of the specimen height and then tested in the three-point bending configuration – see the selected photos in Fig. 1.5. for illustration. Details regarding the evaluation of the fracture tests from various points of view can be found in, for example, (Šimonová *et al.*, 2017a) and (Šimonová *et al.*, 2017b). After the fracture tests had been performed, the fracture surface of each specimen was scanned via a 2D laser profilometer – Fig. 1.4. (right) schematically shows the surface area of the ligament ( $A_{lig}$ ) under investigation. The maximum temperatures within the concrete specimens at different distances from the heated side of the panels are presented in Table. 1.2. These data were obtained via the nonlinear approximation of the temperatures measured by the

thermocouples – see (Rozsypalová *et al.*, 2018) for details. The mean values obtained for several basic mechanical fracture parameters of the concrete specimens presented in (Rozsypalová *et al.*, 2017) are introduced in Table. 1.3.

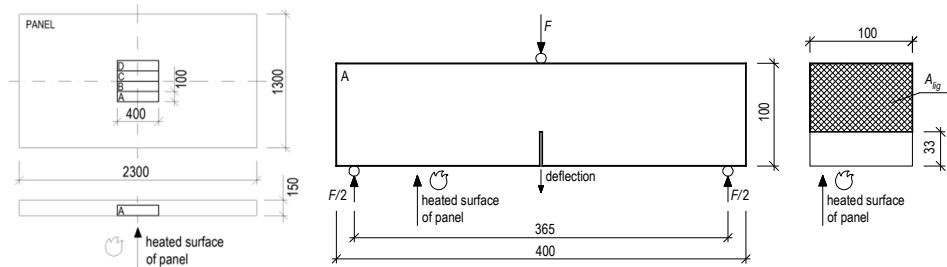


**Fig. 1.4.** Panel diagram and positions of specimens sawn off for fracture experiments (left), configuration of the fracture test in three-point bending and designation of the investigated ligament area

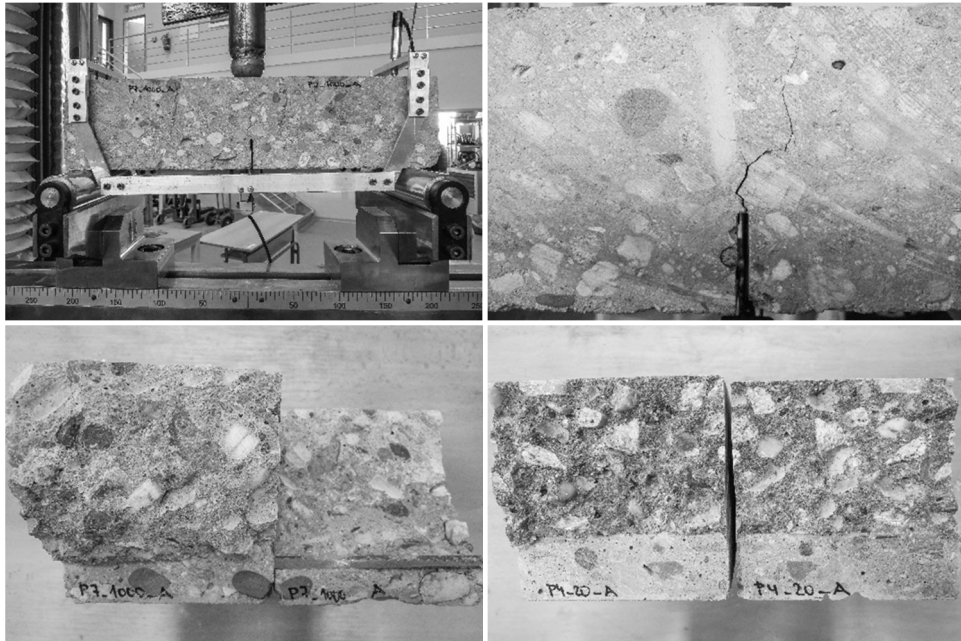


**Fig. 1.5.** Illustration of a fracture test in the three-point bending configuration and detail of the crack path; examples of selected specimens after testing – the ligament of P7\_1000\_A (maximum furnace temperature 1000 °C) and P4\_20\_A (reference specimen)

**Table. 1.2.** Maximum temperature [°C] in specimens at different distances from the heated side of the panel/specimen

Distance [mm]	P4_20	P1_550	P2_600	P3_800	P7_1000
0 (heated side of panel)	20	565	591	777	974
33 (depth of specimen notch)	20	251	293	388	501
100 (upper side of specimen)	20	113	137	168	248

**Table. 1.3.** Mean values obtained for basic mechanical fracture parameters of the concrete specimens

Parameter	Unit	P4_20	P1_550	P2_600	P3_800	P7_1000
Elasticity modulus	GPa	38.0	13.7	9.87	3.91	2.48
Fracture toughness	MPa·m <sup>-1/2</sup>	1.181	0.922	0.938	0.774	0.449
Fracture energy	J·m <sup>-2</sup>	138.1	191.2	198.1	321.8	442.0

## 1.5. Ligament scanning procedure

Optical profilometry is widely used to determine surface roughness and topography in a variety of industrial applications. A number of different target surfaces can be measured and evaluated via this contactless and non-destructive method. Several principal methods, such as triangulation and interference, provide two-dimensional data (line scans) or three-dimensional surface images. A commercially available laser profilometer was used to precisely scan the topography of the concrete specimens in our experiments.

2D laser profilometers generally operate with a semiconductor laser of a defined wavelength and use the laser triangulation principle for two-dimensional profile detection on different target surfaces. The laser beam is enlarged using special lenses to form a static laser line and is projected onto the target surface. The diffusely reflected light from the laser line is replicated on a sensitive sensor matrix by a high-quality optical system and evaluated in two dimensions. In addition to distance information (z-axis), the exact position of each point on the laser line (x-axis) is also acquired by an integrated controller. The obtained values are finally output in a two-dimensional coordinate system that is fixed with respect to the sensor (Micro-Epsilon: Instruction manual, 2D/3D laser scanner). The basic design of a typical 2D laser profilometer is shown in Fig. 1.6.

A mobile laser profilometer (a *scanCONTROL 2750-100* made by Micro-Epsilon) was used in this measurement system. It employs a semiconductor laser with a wavelength of 660 nm (visible red line). The declared minimum resolution is 25 µm and it achieves scanning speeds of up to 4000 profiles per second (with 640 points per profile) (Micro-Epsilon: Instruction manual). It is possible to obtain the surface topography in 3D by moving either the target samples or the laser scanner

itself. In our experimental set-up, the laser scanner is mounted on a tripod and specimen motion under the fixed 2D profilometer is realized by a precise linear motion sliding table with a stepper motor. The designed system is capable of smooth and adjustable specimen motion (smallest step  $2.5\ \mu\text{m}$ ) and supports a maximum specimen weight of 10 kg. Sliding table motion is controlled by a developed microprocessor driver that is linked to the master control PC. The issue of distance selection between the acquired line profiles should be solved with respect to achieving a compromise between the expected measurement accuracy and the amount of processed and evaluated data. In the case of our evaluated surfaces, a distance of  $50\ \mu\text{m}$  between the scanned lines/profiles (shift on the  $y$ -axis) was selected, and the spacing between neighbouring points within one line/profile ( $x$ -axis) was also  $50\ \mu\text{m}$ . Illustrative photos of the experimental set-up in the laboratory are shown in Fig. 1.7.

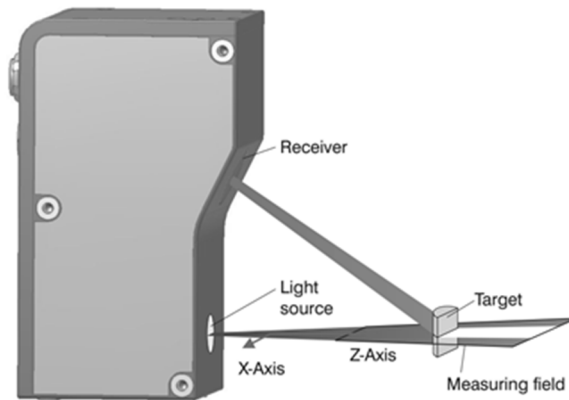


**Fig. 1.6.** The basic design of a typical 2D laser profilometer, taken from (Micro-Epsilon: Instruction manual)

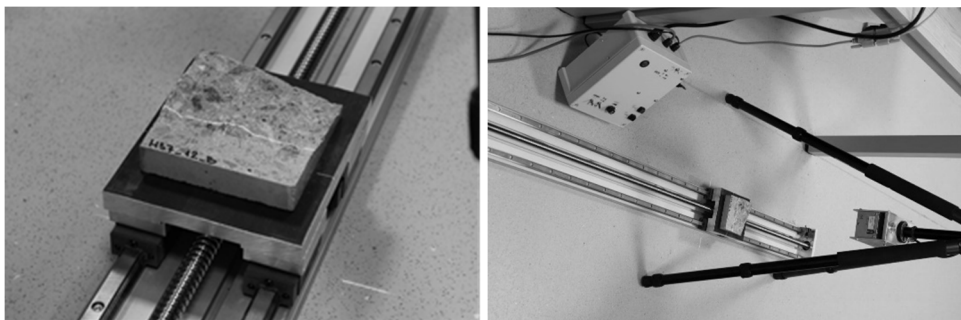


**Fig. 1.7.** Photos from the experimental set-up

The whole experimental set-up is fully automated and the measuring process is controlled by software developed in the MATLAB environment. It allows the control of movements defined specifically for each specimen via the microprocessor driver and continuous profile measurement by the 2D profilometer. The integrated FireWire interface enables complete control of the laser scanner via the computer, as well as high-speed data acquisition. The software also provides pre-processing (profile averaging and basic filtration) of the obtained data, including their storage in the resulting data matrix. After the surface scanning, the final 3D specimen topography can also be displayed using this software (see Fig. 1.8. and Fig. 1.9. for illustration) and some additional operations can be performed (cropping the monitored area, rendering 2D and 3D surfaces, saving results in different data formats, etc.).

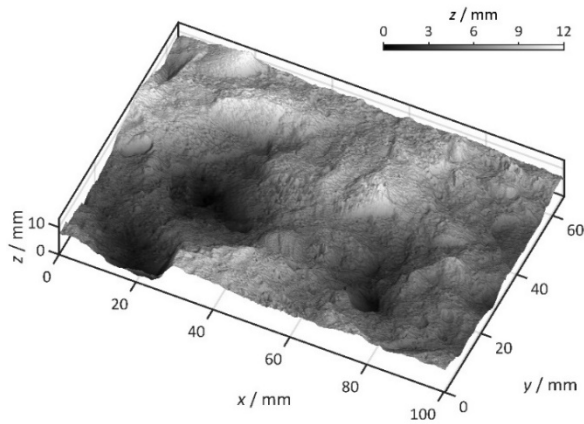


**Fig. 1.8.** 3D topography – specimen P4\_20\_C\_2

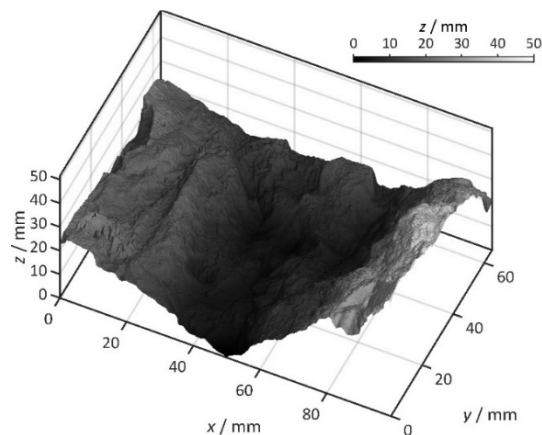


**Fig. 1.9.** 3D topography – specimen P7\_1000\_C\_2

A complex and modular software package was also developed for the post-processing of the measured data. The basic module allows the calculation of some basic surface roughness parameters inspired by technical standards such as ISO 25178, ISO 4287:1997 (Geometrical Product Specifications (GPS) – Surface texture: Profile method – Terms, definitions, and surface texture parameters), etc. The proposed roughness parameters can be evaluated from individual 2D profiles or whole 3D surfaces. Another separate module is focused on the determination of the total fracture area in a selected region of the scanned surfaces. It is solved by a simple algorithm that allows the approximate surface area between the four neighbouring points of the data matrix (z-axis) to be quantified by dividing the resulting pattern in a 3D coordinate system into two triangles. The area of these triangles can be calculated on the basis of Heron's formula or suitably selected vector products. The total fracture area is therefore determined by the sum of the areas of all triangles in the region of interest.

## 1.6. Fractal dimension calculations

The estimation of the fractal dimension of each selected fracture surface section was performed using the walking divider method – see e.g. (Annadhasan, 2012). The procedure for calculating the dimension estimate is to determine how many lines of a given length  $l$  (scale) are required to cover the measured curve. Changing this scale determines how the number of covering lines  $N(l)$  is changed, while for the measured length  $L(l)$  the following applies:  $L(l) = N(l) \cdot l$ . Ideally, the dependence of the number of covering segments given by the expression  $N(l) = a \cdot l^{-D}$  is linear in a logarithmic representation (see Fig. 1.10. for the ligament of specimen P7\_1000\_A2 and a selected section at a distance of 5 mm from the initiation notch), where  $a$  is an unknown constant and a  $D$  is an estimate of the fractal dimension. The result is an expression for the length,  $L(l) = a \cdot l^{1-D}$ . The constants can be obtained by approximating the measured lengths of the curve for the selected scales. The calculated dimension  $D$  estimate for the curves (sections) at different distances  $d$  from the notch for the selected fracture surface P7\_1000\_A2 is illustrated in Fig. 1.11. In this case, the dimensionless value of the fractal dimension is  $D = 1 - (-0.0135) = 1.0135$ .

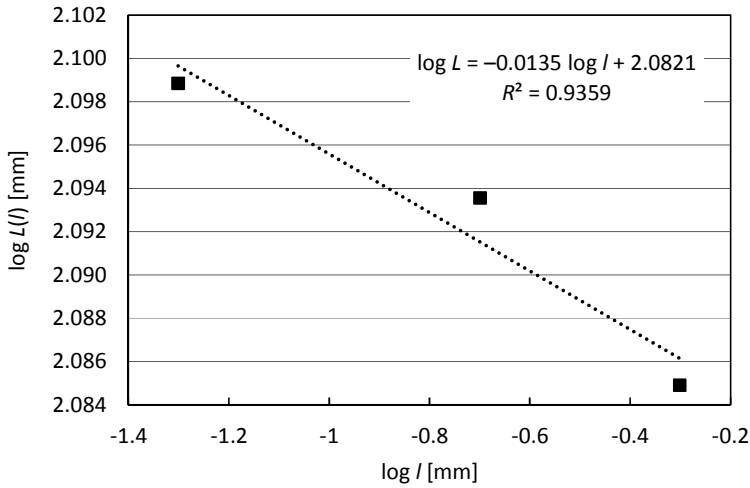


**Fig. 1.10.** Regression line (including coefficient of determination) approximating the points of the logarithm of the length of the curve  $L(l)$  to the logarithm of the length of scale  $l$ , which is the source for determining the fractal dimension of the selected section of the ligament

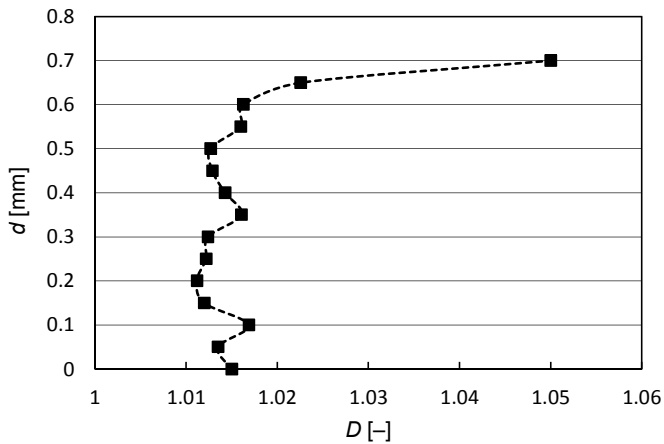


**Fig. 1.11.** Estimated fractal dimension  $D$  along the height  $d$  of the ligament (at different distances from the notch) of specimen P7\_1000\_A2 for 15 selected sections

## 1.7. Results and discussion

### 1.7.1. Primary characterization of ligament roughness

For the primary evaluation of the roughness of the obtained fracture surfaces a procedure was programmed which calculates the roughness parameter  $r$  defined as  $r = L/L_p [-]$ , where  $L$  means the length of the curve representing a section of the fracture surface and  $L_p$  is the length of its projection onto axis  $x$ . The graphs in Fig. 1.12. to Fig. 1.16. show the results of the calculation of ratio  $r$  for the studied specimens (a selected surface for each specimen: A, B, C, and D), while only a carefully selected area of the complete scanned surface was included in the calculation (trimming the edges of the specimen and focusing on the ligament fracture area  $A_{lig}$  only). Basic statistics for all roughness parameters  $r$  are shown in Table. 1.4. This statistical evaluation was based on eight mean values obtained for the parameters  $r$  of each ligament of four specimens after the fracture tests.

**Table. 1.4.** Basic statistics for roughness parameters  $r$  for all tested specimens/panels

Parameter	Unit	P4_20	P1_550	P2_600	P3_800	P7_1000
Mean value	–	1.127	1.173	1.185	1.258	1.265
Standard deviation	–	0.008	0.023	0.029	0.055	0.118
Coefficient of variation	%	0.7	1.9	2.4	4.4	9.4

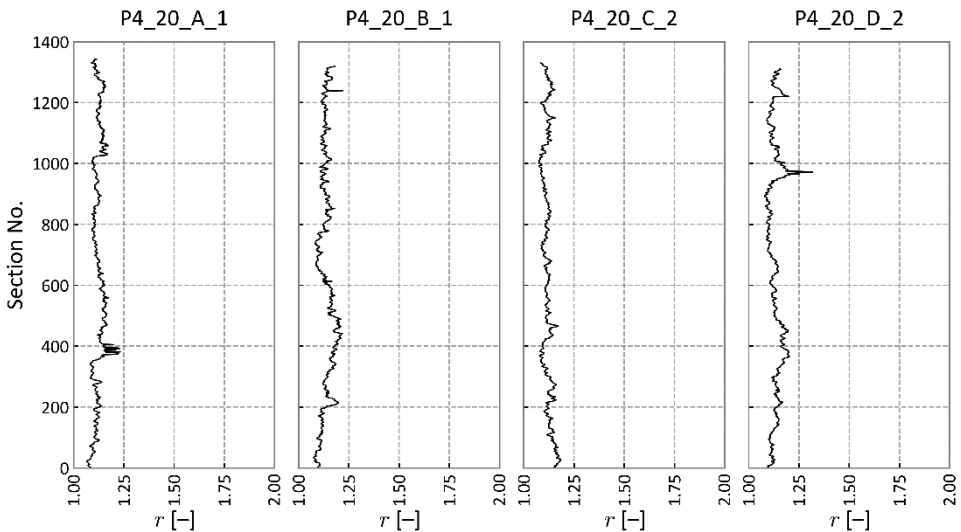


**Fig. 1.12.** The roughness parameter along the height of the ligament after the fracture test (section number) for specimens from the reference panel for 20 °C, i.e. without thermal load

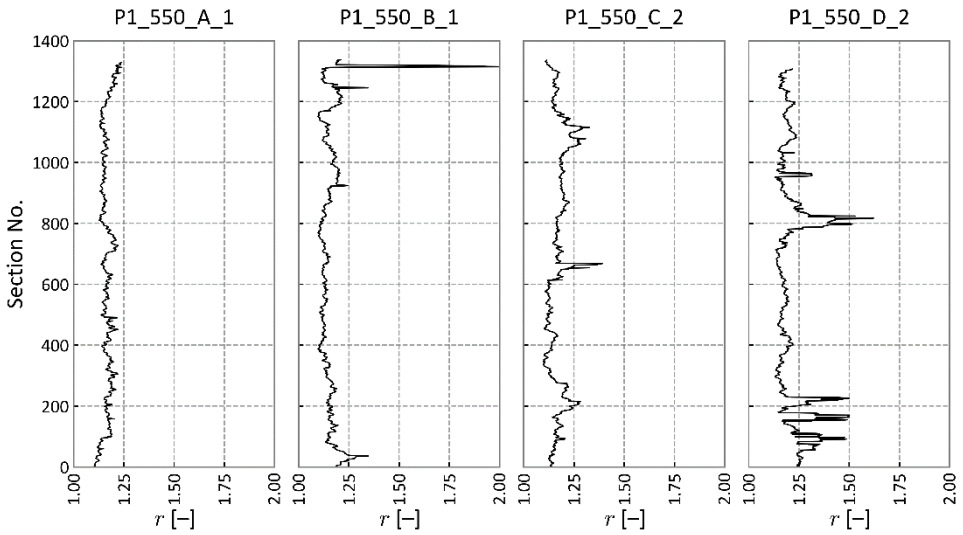


**Fig. 1.13.** The roughness parameter along the height of the ligament after the fracture test (section number) for specimens from the panel thermally-loaded with a nominal maximum furnace gas temperature of 550 °C

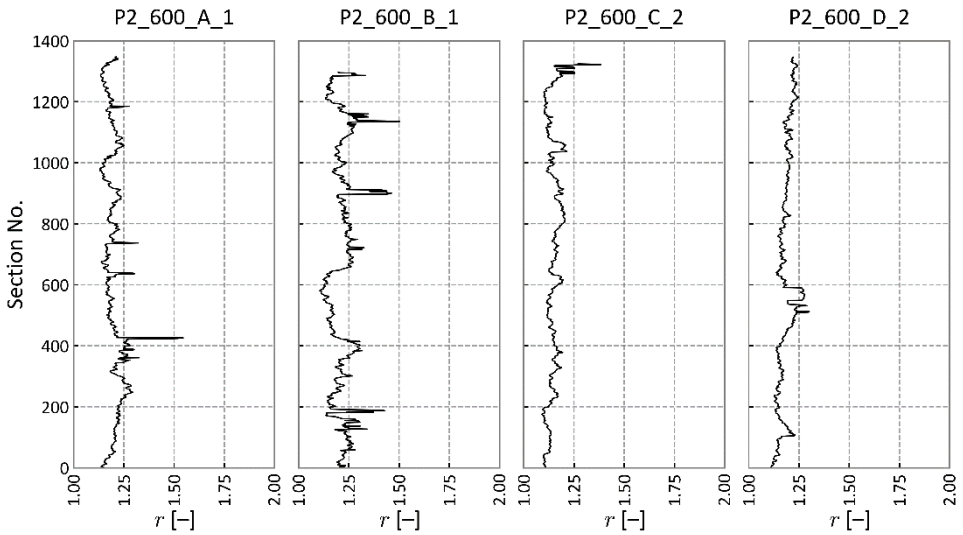


**Fig. 1.14.** The roughness parameter along the height of the ligament after the fracture test (section number) for specimens from the panel thermally-loaded with a nominal maximum furnace gas temperature of 600 °C

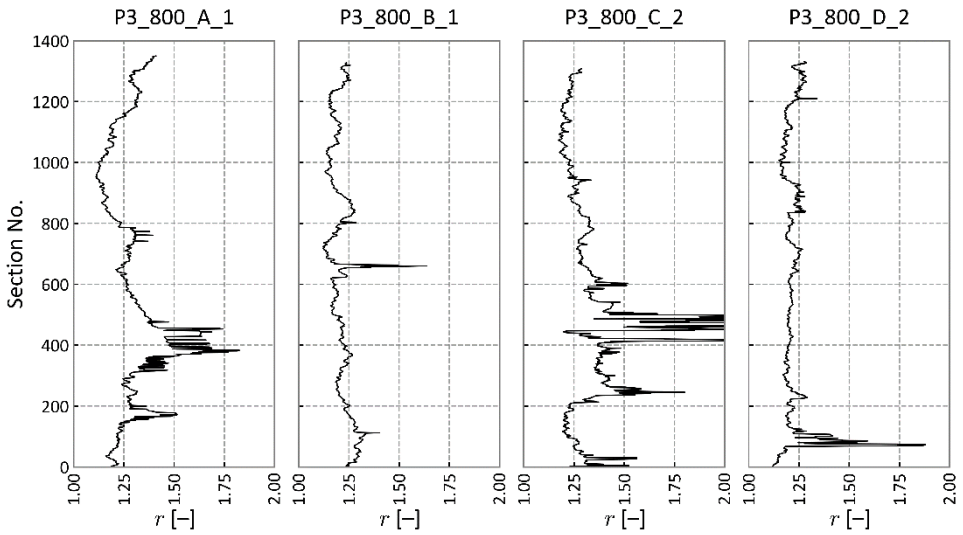


**Fig. 1.15.** The roughness parameter along the height of the ligament after the fracture test (section number) for specimens from the thermally-loaded panel with a nominal maximum furnace gas temperature of 800 °C

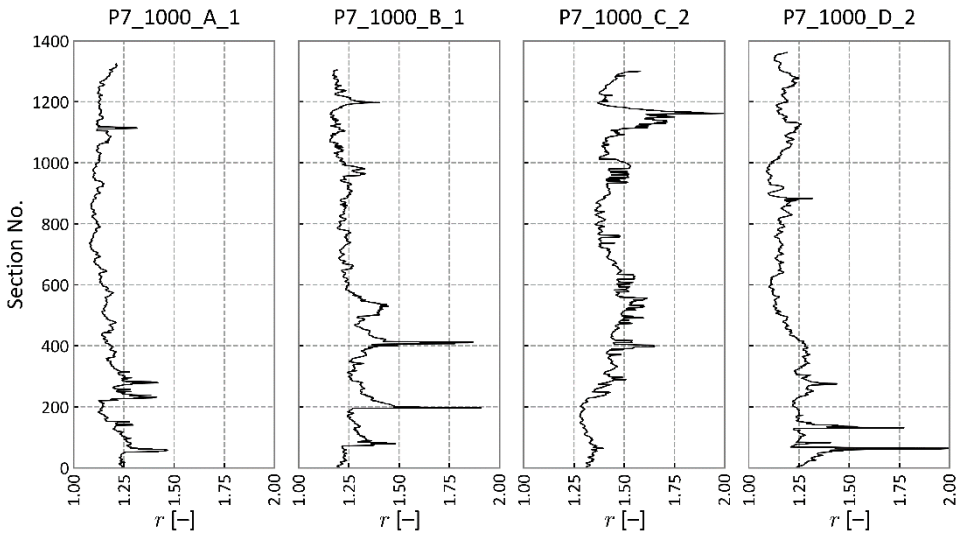


**Fig. 1.16.** The roughness parameter along the height of the ligament after the fracture test (section number) for specimens from the thermally-loaded panel with a nominal maximum furnace gas temperature of 1000 °C

### 1.7.2. Fractal dimensions of ligaments

The procedure for the estimation of the fractal dimension  $D$  of selected fracture surface sections was introduced in the pertinent previous subchapter. Results for all studied fracture surfaces and 14 selected sections of these surfaces at increasing distances from the end of the initial notch are depicted in the following figures. In each figure it is possible to see four particular values for the fractal dimension  $D$  of the section of the fracture surface and a mean value with the range of standard deviation: Fig. 1.17. shows results for specimens from panel P4 (reference panel), while Fig. 1.18. to Fig. 1.21. show results for specimens from panels P1 (nominal maximum gas temperature 550 °C), P2 (600 °C), P3 (800 °C), and P7 (1000 °C), respectively. Global statistics for all the fractal dimension  $D$  measurements (mean values of individual mean values, etc.) are shown in Table. 1.5.

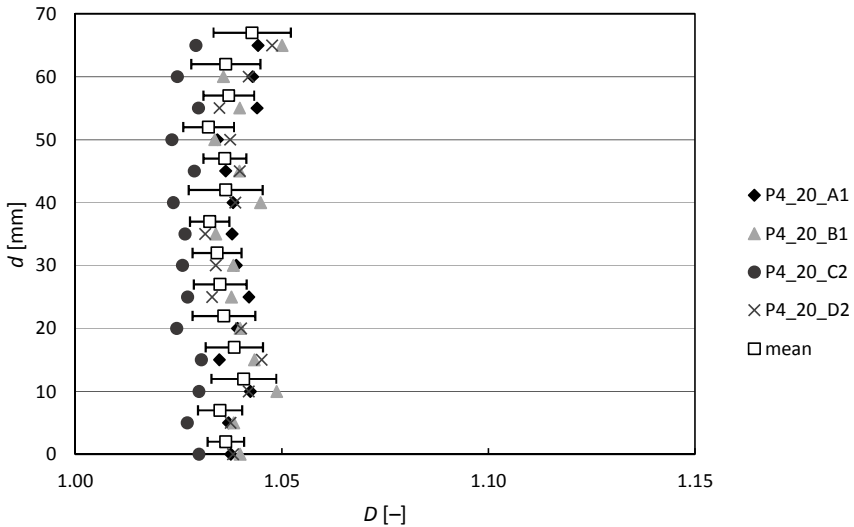


**Fig. 1.17.** Fractal dimension along the height of 4 ligaments P4\_20 for selected line profiles; estimated temperature range between the lower and upper edge of the ligament: 20–20 °C (reference panel)

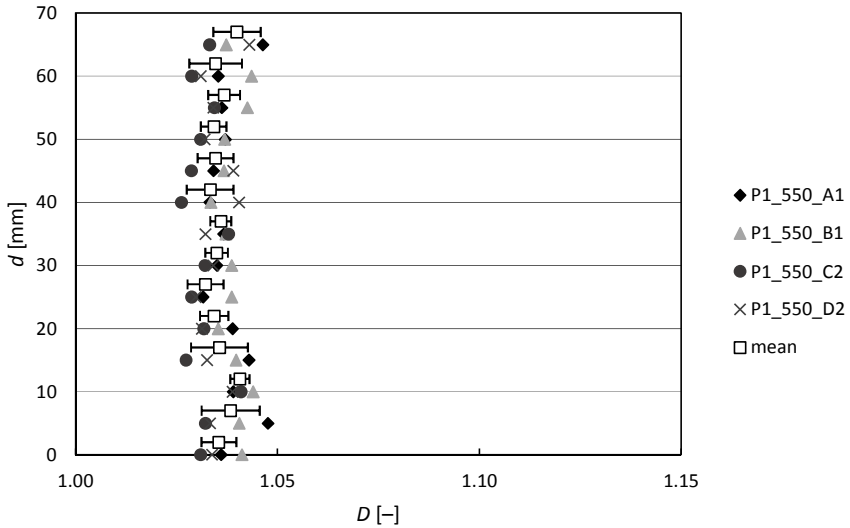


**Fig. 1.18.** Fractal dimension along the height of 4 ligaments P1\_550 for selected line profiles; estimated temperature range between the lower and upper edge of the ligament: 250–115 °C

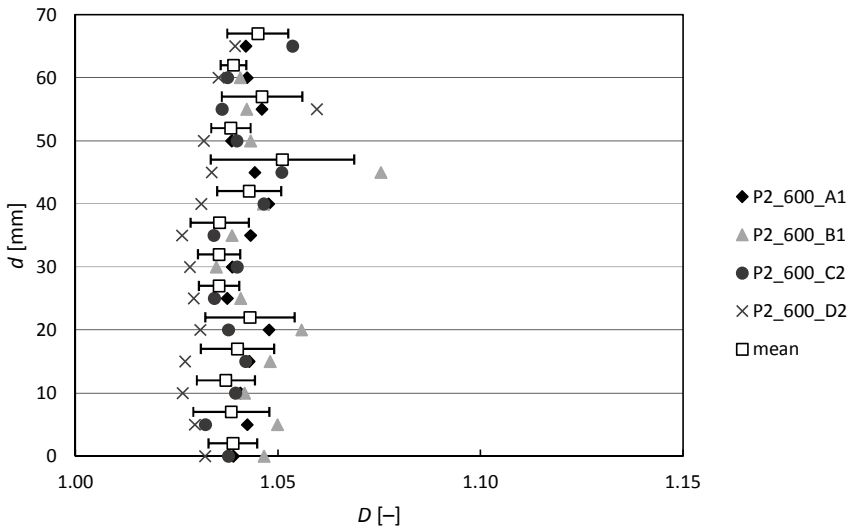


**Fig. 1.19.** Fractal dimension along the height of 4 ligaments P2\_600 for selected line profiles; estimated temperature range between the lower and upper edge of the ligament: 300–140 °C

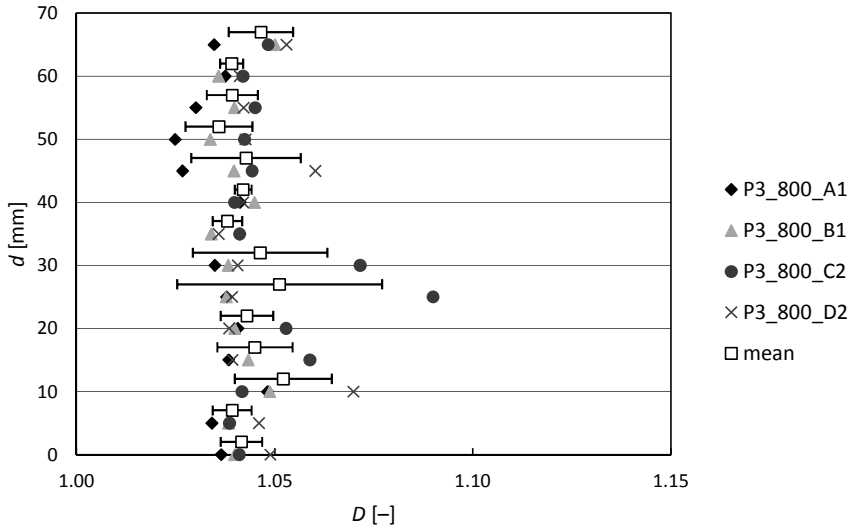


**Fig. 1.20.** Fractal dimension along the height of 4 ligaments P3\_800 for selected line profiles; estimated temperature range between the lower and upper edge of the ligament: 390–170 °C

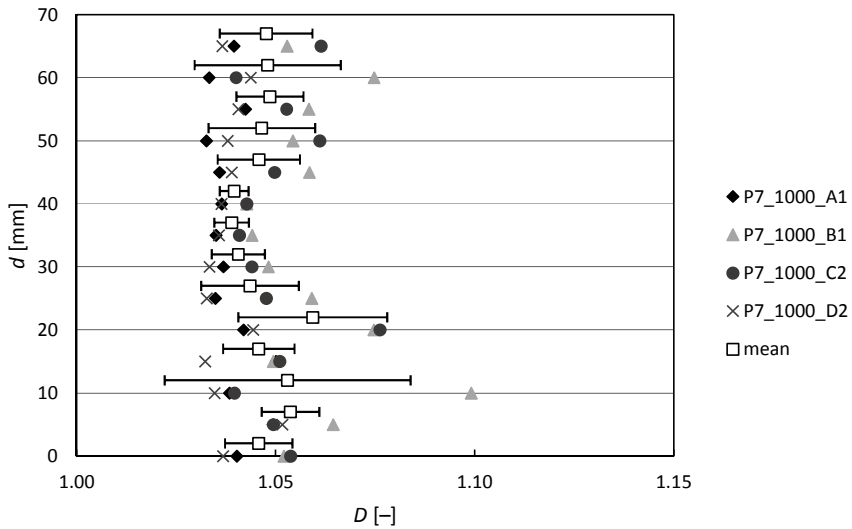


**Fig. 1.21.** Fractal dimension along the height of 4 ligaments P7\_1000 for selected line profiles; estimated temperature range between the lower and upper edge of the ligament: 500–250 °C

**Table. 1.5.** Basic statistical parameters of fractal dimension  $D$  for all tested specimens/panels

Parameter	Unit	P4_20	P1_550	P2_600	P3_800	P7_1000
Mean value	–	1.0364	1.0358	1.0405	1.0431	1.0469
Standard deviation	–	0.00284	0.00242	0.00461	0.00480	0.00564
Coefficient of variation	%	0.27	0.23	0.44	0.46	0.54

### 1.7.3. Correlation among temperature, fracture properties and fractal dimensions

Correlation coefficients among the maximum temperatures, the mean values of selected, previously obtained, mechanical fracture parameters, and the values determined for roughness characteristics are shown in Table. 1.6. – the lower part of the symmetrical correlation matrix. The maximum temperatures correspond to three distances from the heated surface of the concrete specimens during fracture tests in three-point bending. In Table. 1.6. below the following notation is used to refer to parameters:

- $T_{max, d0}$  – the maximum temperature at the heated side of the concrete panel ( $d = 0$  mm), i.e. at the bottom side of the specimens,
- $T_{max, d33}$  – approximation of the maximum temperature at distance  $d = 33$  mm, equal to the depth of the specimen notch,
- $T_{max, d100}$  – approximation of the maximum temperature at distance  $d = 100$  mm, i.e. at the upper side of the specimen,
- $E$  – modulus of elasticity,
- $K_{Ice}$  – effective fracture toughness,
- $G_F$  – specific fracture energy,
- $r$  – roughness parameter,
- $D$  – fractal dimension.

**Table. 1.6.** Correlation coefficients [–] among the maximum temperatures, mechanical fracture parameters, and roughness characteristics

	$T_{max, d0}$	$T_{max, d33}$	$T_{max, d100}$	$E$	$K_{Ice}$	$G_F$	$r$	$D$
$T_{max, d0}$	1							
$T_{max, d33}$	1.00	1						
$T_{max, d100}$	0.98	0.99	1					
$E$	–0.97	–0.96	–0.92	1				
$K_{Ice}$	–0.94	–0.95	–0.98	0.84	1			
$G_F$	0.87	0.91	0.93	–0.76	–0.97	1		
$r$	0.93	0.95	0.93	–0.89	–0.92	0.94	1	
$D$	0.81	0.87	0.90	–0.74	–0.89	0.94	0.91	1.00

#### 1.7.4. Discussion of the achieved results

The achieved results allow a number of conclusions to be drawn. These are conclusions about the influence of thermal loading on the roughness of fracture surfaces, the direction of one-side heating and distance from the heated surface, and on the values of mechanical fracture parameters. The possibility of characterizing fracture surface roughness also appears to be an important result. The dependency of the roughness parameter  $r$  and also fractal dimension  $D$  of the fracture surface section on exposure to high temperatures and section position (distance  $d$  from the heated surface) was presented. It has been shown that exposure to high temperatures causes increased variability in the roughness parameter as well as the fractal dimension values and a slight increase in their mean values; an exception to this tendency can be seen in the case of the fractal dimensions of sections of the fracture surfaces of specimens after thermal loading at a nominal maximum temperature of 550 °C, which clearly shows the lowest mean values and variability of fractal dimensions. In some cases, a more significant change in the fractal dimension  $D$  was visible near the upper part of the specimen (the section at the highest distance from the notch), which may be related to the fact that the material was under higher compressive stress in this part.

Among all the results (mean values of parameters) a high degree of correlation was shown – the lowest absolute correlation coefficient was approximately 0.74 [–], which means that the correlation indicates a strong to (almost) perfect linear relationship between pairs of parameters in all cases, whether positive or negative.

The modulus of elasticity  $E$  shows an almost perfect negative correlation with maximum temperature, the correlation in absolute value slightly decreasing with distance from the heated surface. This corresponds well to the fact that the value of the elastic modulus is calculated from the linear initial branch of the diagram of load versus midspan deflection.

A similar almost perfect negative correlation at maximum temperature was shown by effective fracture toughness  $K_{ice}$ . Its value expresses a degree of non-linearity before reaching the maximum load in the load versus midspan deflection diagram, thus reflecting some initiation of concrete damage in front of the notch – the initiation of the fracture process zone. From this perspective, it is adequate that the absolute value of the correlation coefficient increases slightly with the distance from the notch.

Specific fracture energy  $G_F$  is calculated from the work of fracture in relation to the originated concrete test specimen surfaces and showed a very strong positive correlation with the maximum applied temperature. As in the case of fracture toughness  $K_{ice}$ , it is again satisfactory that the value of the correlation coefficient increases slightly with the distance from the notch.

Fractal dimension  $D$  shows a very strong correlation with maximum temperature and at the same time with both concrete fracture parameters – negative in the case of effective fracture toughness and positive in case of specific fracture energy. With higher maximum temperatures, the concrete becomes brittle in relation to the response around the top of the load versus midspan deflection diagram, but becomes more tough (ductile) due to the formation of a larger and more complicated fracture process zone – thus increasing resistance against the principal crack propagation of the concrete and correspondingly forming a more complicated fracture surface with a higher fractal dimension.

It has also been shown that, in the absence of a fractal dimension  $D$ , the fracture surface can be characterized very well in a similar (and easier) way by the roughness parameter  $r$  – the correlation coefficient between these parameters was 0.91 [–].

## **1.8. Conclusions**

In the chapter, the possibilities of characterizing the roughness of the ligament of a concrete specimen after fracture testing by the fractal dimension were shown. The fracture surfaces of specimens taken from thermally-loaded experimental panels were analysed. It was shown that fracture surface roughness significantly depends on the thermal load, and also that the estimated fractal dimension shows dependence on the distance of the selected section of ligament from the notch, i.e. from the heated side of the specimens.

All of the above-presented analyses allow the following conclusions to be drawn:

- concrete surfaces after fracture tests have a fractal nature;
- the fractal dimension most suitably describes fracture surface roughness;
- the application of thermal loading to concrete causes changes in basic mechanical fracture parameters;
- fractal dimension highly correlates with all investigated mechanical fracture parameters;
- the roughness parameter is a perfect approximation of fractal dimension;
- the spatial temperature gradient significantly affects fracture parameters;
- the temperature gradient very slightly influences the fractal dimension of a fracture surface, and its variability;
- it is open to discussion as to whether and how different maximum temperatures should be distinguished along a ligament according to its measured fractal dimension.

## Acknowledgement

Financial support provided by the Czech Science Foundation (GACR) under project No. 19-09491S (MUFRRAS) is gratefully acknowledged. This paper was produced under the “National Sustainability Programme I” project “AdMaS UP – Advanced Materials, Structures and Technologies” (No. LO1408) supported by the Ministry of Education, Youth and Sports of the Czech Republic and Brno University of Technology.

## References

- AdMaS Science Centre (no date). Available at: <http://www.admas.eu/>.
- Aïtcin Pierre-Claude, M. S. (2011) *Sustainability of Concrete*. 1st edn. London: CRC Press. doi: <https://doi.org/10.1201/9781482266696>.
- Annadhasan, A. (2012) ‘Methods of Fractal Dimension Computation’, *IRACST - International Journal of Computer Science and Information Technology & Security*.
- Bazant, Z. P. and Planas, J. (1998) *Fracture and size effect in concrete and other quasibrittle structures*. Boca Raton and London: CRC Press.
- Babadagli, T. and Develi, K. (2003) ‘Fractal characteristics of rocks fractured under tension’, *Theoretical and Applied Fracture Mechanics*. doi: 10.1016/S0167-8442(02)00139-8.
- Borodich, F. M. (1999) ‘Fractals and fractal scaling in fracture mechanics’, *International Journal of Fracture*.
- Carpinteri, A., Chiaia, B. and Invernizzi, S. (1999) ‘Three-dimensional fractal analysis of concrete fracture at the meso-level’, *Theoretical and Applied Fracture Mechanics*. doi: 10.1016/S0167-8442(99)00011-7.
- Carpinteri, A., Chiaia, B. and Cornetti, P. (2001) ‘A scale-invariant cohesive crack model for quasi-brittle materials’, *Engineering Fracture Mechanics*. doi: 10.1016/S0013-7944(01)00085-6.
- Carpinteri, A. and Puzzi, S. (2006) ‘A fractal approach to indentation size effect’, *Engineering Fracture Mechanics*. doi: 10.1016/j.engfracmech.2006.04.020.
- Carpinteri, A. and Lacidogna, G. (2008) *Acoustic Emission and Critical Phenomena From Structural Mechanics to Geophysics*. 1st edn. London: CRC Press. doi: <https://doi.org/10.1201/9780203892220>.
- Edelman, M., Macau, E. E. N. and Sanjuan, M. A. F. (2018) *Chaotic, Fractional, and Complex Dynamics: New Insights and Perspectives*. Springer International Publishing AG. doi: 10.1007/978-3-319-68109-2\_1.
- EN 1991-1-2:2002/AC (2013) *Eurocode 1: Actions on structures – Part 1-2: General actions – Actions on structures exposed to fire*. Brussels: CEN.
- Ficker, T. (2007) ‘Dimension of Fracture Surfaces’, *Acta Polytechnica*, 46(6), pp. 27–30.

- Ficker, T. (2008) 'Fractal strength of cement gels and universal dimension of fracture surfaces', *Theoretical and Applied Fracture Mechanics*, 50(2), pp. 167–171. doi: 10.1016/j.tafmec.2008.07.004.
- John, A. P. and Li, L.-Y. (2011) *Fire Safety Engineering Design of Structures*. Boca Raton: CRC Press.
- Kozlov, H. V., Burya, O. I. and Aloev, V. Z. (2004a) 'Application of fractal fracture mechanics to polymers and polymeric composites', *Materials Science*. doi: 10.1007/s11003-005-0066-1.
- Kozlov, H. V., Burya, O. I. and Aloev, V. Z. (2004b) 'Application of fractal fracture mechanics to polymers and polymeric composites', *Materials Science*, 40(4), pp. 491–496. doi: 10.1007/s11003-005-0066-1.
- Mandelbrot, B. B. (1982) *The fractal geometry of nature*, *New Scientist*. New York: Freeman.
- Mandelbrot, B. B., Passoja, D. E. and Paullay, A. J. (1984) 'Fractal character of fracture surfaces of metals', *Nature*, 308, pp. 721–722. doi: 10.1038/308721a0.
- Mecholsky, J. J., Passoja, D. E. and Feinberg-Ringel, K. S. (1989) 'Quantitative Analysis of Brittle Fracture Surfaces Using Fractal Geometry', *Journal of the American Ceramic Society*, 72(1), pp. 60–65. doi: 10.1111/j.1151-2916.1989.tb05954.x.
- Micro-Epsilon: 2D/3D laser scanner (laser profile sensors)* (no date). Available at: <https://www.micro-epsilon.com/download/products/cat--scanCONTROL--en-us.pdf>.
- Mourot, G. *et al.* (2005) 'Anomalous scaling of mortar fracture surfaces', *Physical Review E - Statistical, Nonlinear, and Soft Matter Physics*, 71(1), pp. 1–7. doi: 10.1103/PhysRevE.71.016136.
- Nevile, A. M. (2011) *Properties of Concrete*. Harlow: Pearson Education Limited.
- Passoja, D. E. and Amborski, D. J. (1978) 'Fractal profile analysis by Fourier transform methods', *Microstructural Science*, 6, pp. 143–148.
- RILEM TC 129-MHT (1997) 'TC 129 MHT: Test methods for mechanical properties of concrete at high temperatures: Part 6: Thermal strain', *Materials and Structures*, 33, pp. 17–21.
- Rozsypalová, I. *et al.* (2017) 'Mechanical Fracture Parameters of Concrete Specimens from One-Side-Heated Panel', in *SP Report 2017:43 Proceedings from the 5th International Workshop on Concrete Spalling*. Borås: RISE Research Institutes of Sweden AB, p. 105–111.
- Rozsypalová, I. *et al.* (2018) 'Mechanical fracture parameters of concrete exposed to high temperatures related to approximation of temperature fields in experimental panels', in *Proceedings for the 2018 fib Congress held in Melbourne*. Lausanne: Fédération internationale du béton (fib), p. 670–671.
- Shah, S. P., Swartz, S. E. and Ouyang, C. (1995) *Fracture mechanics of structural concrete: applications of fracture mechanics to concrete, rock, and other*

*quasi-brittle materials*. New York: John Wil. and Sons.

- Šimonová, H., Trčka, T., *et al.* (2018) 'Detailed Determination of Mechanical Fracture Parameters of Concrete after Fire Experiments', in *Solid State Phenomena: 24th Concrete Days*. Switzerland: Trans Tech Publications, p. 220–225.
- Šimonová, H., Rozsypalová, I., *et al.* (2018) 'Thermal Analysis of Concrete from Panels Subjected to Fire Experiments', in *Solid State Phenomena: 24th Concrete Days 2017*. Switzerland: Trans Tech Publications, p. 47–52.
- Wang, Y. *et al.* (2017) *Performance-Based Fire Engineering of Structures*. Boca Raton: CRC Press.